UCRL-JC-121584
PREPRINT

Control of Laser Plasma Instabilities in Hohlraums

W. L. Kruer

This paper was prepared for submittal to the
1995 La Jolla Summer School
La Jolla, California
August 8-18, 1995

December 18, 1996

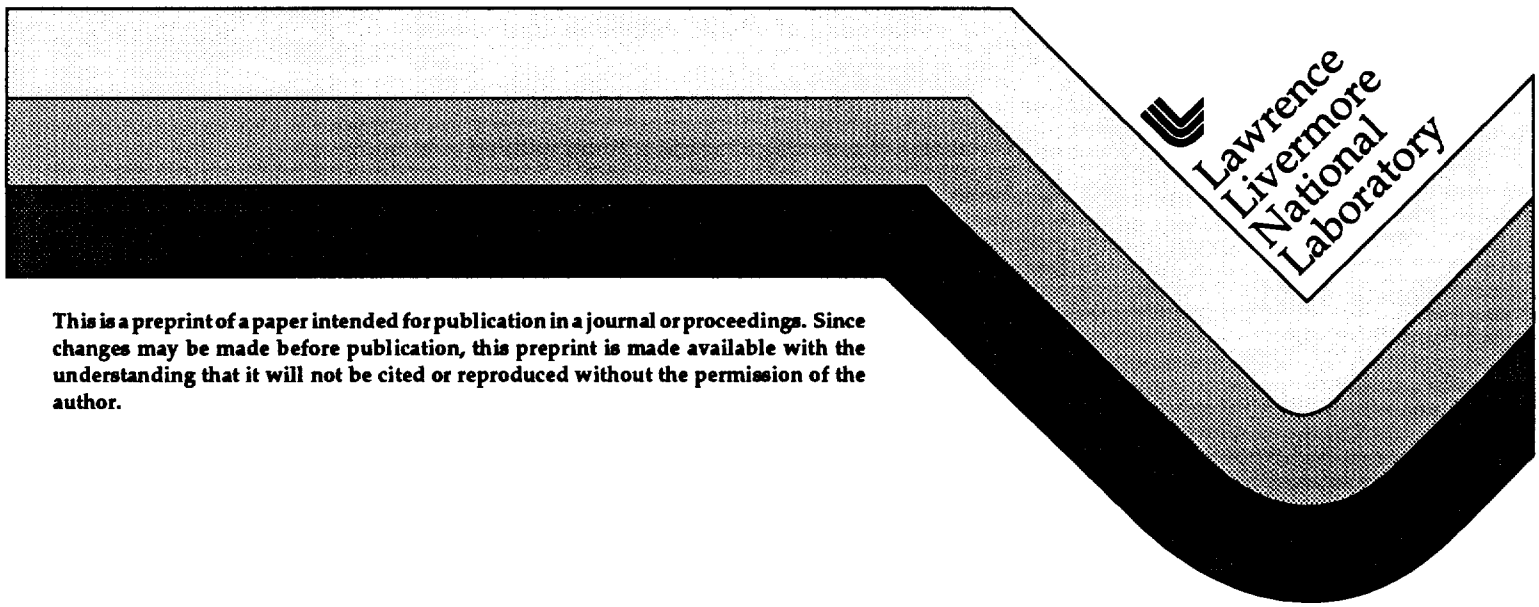

Control of Laser Plasma Instabilities in Hohlraums

William L. Kruer
Lawrence Livermore National Laboratory

Abstract

Laser plasma instabilities are an important constraint on the operating regime for inertial fusion. Many techniques have been developed to control the various laser-driven instabilities. Experiments with long scale length plasmas are testing these instability levels, the nonlinear regimes, and the control mechanisms.

1. Introduction

In the indirect approach[1] to inertial fusion laser light is used to irradiate the interior of a hohlraum. The simplest example of a hohlraum is a gold cylinder with holes in the ends, as show in Figure 1. On striking the high Z wall, the light efficiently converts into x-rays, which are used to implode a capsule in the center of the hohlraum. To obtain sufficient irradiation symmetry on the capsule, it is necessary to retard the motion of the dense high Z wall plasma, where the x-rays are primarily generated. Hence, the hohlraum is filled with a low Z gas, which rapidly turns into a hot plasma. The pressure of this hot plasma slows the motion of the dense high Z plasma wall.

Figure 2 shows some typical plasma and irradiation conditions for an ignition-scale hohlraum. In this case, a hohlraum with a length of 9.5mm and a diameter of 5.5mm is irradiated with 1.35MJ of 0.35μm light configured in inner and outer cones. The time history of the irradiation is shown in Figure 2a. Contours of electron density, temperature and laser intensity at the time of peak powers are shown in Figures 2b, 2c, and 2d. Note the extensive region of the He H plasma in the laser channel. Its density is about $0.1n_{cr}$ (the critical density), its electron temperature is about 5 keV, and its characteristic size L is about 3-5mm. This low Z plasma connects onto a a high Z Au plasma whose density ranges from

about $0.1n_{cr}$ up to greater than n_{cr} in approximately 300μm. The laser absorption primarily occurs in this region. The laser intensity is typically $1-2x10^{15}\frac{W}{cm^2}$.

The laser light absorption is very efficient in the dense, high Z plasma which is quite collisional. For example, the inverse bremsstrahlung absorption length in an Au plasma with a density of a $0.5n_{cr}$ and a temperature of 3keV is only about 30μm. The concern is excitation of laser-driven instabilities[2] in the large region of low density plasma before the light is efficiently absorbed. These instabilities include stimulated Raman and Brillouin scattering and laser beam filamentation due to either ponderomotive or thermal effects. The stimulated scattering instabilities can be most simply characterized as the resonant decay of the intense light wave into a scattered light wave plus either an ion acoustic wave (SBS) or an electron plasma wave (SRS). Filamentation represents the growth of intensity modulations in a laser beam associated with either ponderomotively or thermally-driven density modulations transverse to the beam. The stimulated scattering instabilities can reduce the absorption efficiency or change its location. In addition, superthermal electrons can be generated by the electron plasma waves associated with SRS. If sufficiently energetic, these can preheat the capsule. Tolerable levels of stimulated scattering are about 10-20%. Laser beam filamentation can introduce other instabilities by enhancing the intensity and can lead to beam spraying and deflection. It is prudent to avoid filamentation.

Laser-plasma instabilities provide an important constraint for target design. Since the instability growth depends on intensity, we must limit the intensity used in the target designs. This constraint is illustrated in Figure 3, which denotes the operating regime[3] for an ignition target in laser power versus energy space. The minimum energy is roughly 1MJ. There is a lower power (intensity), which is determined by hydrodynamic instability of the imploding capsule. The upper band is set by laser-plasma instabilities. An improved understanding of laser-plasma instabilities and their control is extremely valuable, both to specify this upper boundary with greater confidence and to relax this constraint as much as possible.

The laser-driven instabilities depend on laser wavelength, intensity and coherence as well as on plasma composition, density, temperature and inhomogenity[4]. Laser wavelength is a very key parameter. As the wavelength is decreased, the plasma is more collisional, the instabilities more weakly driven, and

the plasma fills the hohlraums to a lower fraction of the critical density (which also weakens the instabilities). Current target designs use 0.35μm laser light, which has proved to date sufficiently short to avoid[2] the severe instability generation found in early hohlraums irradiated with 1.06μm light. Here we will discuss some other techniques for instability control.

2. Control of Laser Beam Filamentation

Progress has been made in understanding and controlling laser beam filamentation. This filamentation occurs because a region of increased laser intensity locally depresses the plasma density either via the ponderomotive force or the thermal force (i,e., that due to the pressure increase associated with the higher temperature). The depression in plasma density acts to focus the light, thereby increasing the intensity fluctuation. Filamentation describes the unstable growth of infinitesimal modulations. In practice, there are significant hot spots in the laser beam and the physical process is more appropriately characterized as hot spot self-focusing.

Spatial and temporal incoherence in the laser beam can suppress filamentation and hot spot self-focusing. Let's first consider spatial incoherence as introduced by the use of random phase plates[5] (RPP). These convert a coherent beam into many random phased beamlets which are then overlapped. The resulting intensity pattern is described in terms of speckles, which have a characteristic radius of $r_\perp = f\lambda_o$ and length $\ell_{sp} \cong 8f^2\lambda_o$, where f is the f number of the focusing lens and λ_o is the wavelength. The radius and speckle length simply correspond to the correlation length in the directions transverse and parallel to the direction of propagation. The speckles have a known distribution[6] of intensities. For example, about 5% of the beam energy is in speckles with an intensity ≥ 5 times the average intensity.

The suppression of ponderomotive filamentation can be illustrated by considering the self-focusing of a speckle. Crudely treating a speckle as an isolated hot spot, its self-focusing length (ℓ_{SF}) is

$$\ell_{SF} \cong 2r_\perp \frac{\omega_o}{\omega_{pe}} \frac{v_e}{v_{os}}, \qquad (1)$$

where ω_o (ω_{pe}) is the laser light (electron plasma) frequency and v_{os} (v_e) is the electron oscillatory (thermal) velocity. Stabilization requires that $\ell_{SF} \le \ell_{SP}$, giving

$$f \le \frac{1}{8}\left(\frac{n_{cr}}{n}\frac{\Theta_{keV}}{I_{16}\lambda_{\mu m}^2}\right)^{1/2}. \qquad (2)$$

Here n is the electron plasma density, n_{cr} the critical density, Θ_{keV} the electron temperature in keV, I_{16} the laser intensity in units of $10^{16}\frac{W}{cm^2}$, and $\lambda\mu m$ the wavelength in microns. The same scaling can be obtained in various ways,[7] such as $K\ell_{SP} \le 1$ or $r_\perp \le \lambda_{max}$, where K is the spatial gain of filamentation and λ_{max} the most unstable wavelength.

Temporal incoherence gives additional stabilization. Physically, the effect of bandwidth is to move the speckles before the density perturbation forms. Additional suppression then requires

$$t_c < \frac{f\lambda_o}{c_s}, \qquad (3)$$

where $t_c = \frac{1}{\Delta\nu}$, $\Delta\nu$ is the bandwidth, λ_o the wavelength, and c_s the sound speed. A. Schmitt was the first to show this additional stabilization[8] in simulations of filamentation using the so-called induced spatial incoherence scheme to smooth the laser beam. Similar results have been shown in F3D simulations[7] at Livermore using smoothing by spectral dispersion.

Based on these considerations, some temporal incoherence is desirable for the National Ignition Facility (NIF). The use of RPP alone does not appear to give enough stabilization. Let's consider some characteristic hohlraum parameters: $I = 2x10^{15}\frac{W}{cm^2}$, $\lambda_o = 0.35\mu m$, $n = 0.1n_{cr}$ and $\theta_e = 4keV$. Then Equation 2 gives $f \le 5$, whereas the effective f number for NIF is ≥ 8. According to Equation 3, the added suppression can be obtained by using SSD with 3Å bandwidth. Then $t_c \cong 3ps$, whereas $\frac{r_o}{c_s} \cong 6ps$. Of course, temporal incoherence is also needed for the direct drive option.

The experimental evidence for suppression of filamentation by beam smoothing is somewhat indirect. Usually reductions in the levels of SRS and SBS are observed[9], which are attributed to reduced filamentation. Recently there have been experiments illustrating some consequences of filamentation, such as laser beam spraying[10, 11] and deflection.[12, 13] There is also increased interest in effects such as plasma-induced beam smoothing[11], which is due to interaction with density modulations in the plasma. A better understanding of the role of plasma flow[14] and nonstationary behavior[15], the interaction with reflected waves, and the role of thermal filamentation[16] in the Au plasma is needed.

3. Reducing stimulated Brillouin scattering

Some recently investigated mechanisms to control SBS include plasma composition and long wavelength modulations. Both these mechanisms can be illustrated via discussion of the damped ion wave model of SBS, which is appropriate for large, weakly inhomogeneous plasmas. In this model, the maximum spatial gain rate for SBS is

$$K \equiv \frac{k_o}{8}\left(\frac{v_{os}}{v_e}\right)^2\left(\frac{\omega_{pe}}{\omega_o}\right)^2 / \left(\frac{\nu_i}{\omega_i}\right), \tag{4}$$

where k_o is the laser light wave number, ν_i is the ion wave energy damping rate, and ω_i is the ion wave frequency. Note that the spatial gain rate is inversely proportional to the ion wave damping.

It is well-known that the ion wave damping can be strongly enhanced[17] by the addition of hydrogen to the plasma. Imagine an ion acoustic wave in a Carbon plasma, and change the composition to include a small percentage of protons at the same temperature. The frequency of the acoustic wave is primarily determined by the heavy background carbon atoms, but the Landau damping is increased by the lighter, faster protons. Even nonlinearly, one expects a reduced ion wave amplitude since the protons more readily interact with the wave. For example, the condition for trapping of even a cold proton is

$$\frac{Z_H e\phi}{M_H} = \frac{Z_c \theta_e}{M_c}, \tag{5}$$

where Z_H (M_H) is the charge state (mass) of a hydrogen atom, Z_c (M_c) is that of a carbon atom, and ϕ is the potential associated with the ion wave. Approximating $\frac{e\phi}{\theta e} \cong \frac{\delta n}{n}$, it is clear that the density fluctuation δn is reduced by a factor of two

$\left(\text{i.e.}\,\frac{M_H Z_c}{M_c Z_H}\right)$. Much greater amplitude reductions take place for ion trapping in a warm plasma.

Simulations[18] using a 1D particle ion, fluid electron code show a strong reduction of SBS by both linear and nonlinear processes when protons are added. Figure 4 shows the calculated reduction in back reflection found in some representative simulations in which $I = 3\text{x}10^{15}\frac{W}{cm^2}$, $\lambda_o = 0.35\mu m$, $n = 0.1 n_{cr}$, $T_e = 3keV$, and $\frac{T_e}{T_i} \cong 5$. Note the reduction in reflectivity as the hydrogen percentage (by atom fraction in this plot) is varied. Note that the reflection actually goes up again as the plasma becomes entirely protons, since the phase velocity of the ion wave then increases.

A similar reduction of SBS by addition of hydrogen has been observed in UCLA experiments[19] using 10.6μm light and low density plasmas. Figure 5 shows the reduction in back reflection observed in these experiments as a function of the hydrogen percentage. More recently, a significant reduction of SBS by addition of hydrogen has been observed in experiments with hotter, denser plasmas more characteristic of the NIF targets. Both gas bag[20] and hohlraum plasmas[21] were used in these experiments.

SBS can also be reduced[22] by long wavelength modulations in the plasma. Physically, the gain is reduced because the resonance is detuned. Again the damped ion wave model can be used to show the effect. The spatial gain rate is

$$K = K_{max} / \left[1 + 4\left(\frac{\Delta\omega}{\nu_i}\right)^2\right], \qquad (6)$$

where K_{max} is the maximum rate for perfect tuning and $\Delta\omega$ is the frequency shift. If we consider a long wavelength velocity modulation with amplitude δv and wavenumber $\bar{k} << k$ (the wave number of the ion wave),

$$\Delta\omega = k\delta v \sin \bar{k}x. \qquad (7)$$

Averaging the gain over this modulation gives

$$\int K dx = K_{max} L / \sqrt{1 + 4\alpha^2}, \qquad (8)$$

where $\alpha = \frac{\delta v}{c_s}\frac{\omega_i}{\nu_i}$ and L is the plasma length. For a sound wave, $\frac{\delta v}{c_s} \cong \frac{\delta n}{n}$, where δn is the associated density fluctuation. Note that sizable reductions in gain can

occur for a modulated plasma. For example, for $\alpha = 2$, the spatial gain coefficient is reduced by over a factor of 4.

Modulations have been postulated to at least partially explain the low SBS gains recently measured in experiments[23] with crossing laser beams. There are many sources for such modulations, including filamentation of unsmoothed heater beams, hydrodynamic fluctuations associated with plasma formation or, say, collapse of electron plasma waves driven by SRS. This last source of modulations could help account for the cross talk between SBS and SRS to be discussed shortly. Finally such modulations might be intentionally created by structuring the plasma, as suggested by B. MacGowan.

Quantitative calculations of the nonlinear levels of SBS are an ongoing challenge. Simulations show that intrinsic distortions of the ion distribution function is an important effect. For high Z plasmas (even Xe and H mixtures), ion-ion collisions play a significant role by strongly reducing these distortions in the nonlinear state.[24] Long wavelength modulations matter, as just discussed. Finally, multi-dimensional effects such as scattering of ion waves in angle can play a significant role. Only ion waves with well-defined wave numbers are effective in scattering the incident laser light. Hence any coupling of these ion waves into other wave numbers clearly reduces SBS. In three dimensions, the volume of wave number space for ion waves which do not resonantly scatter the laser light greatly increases. 2-D[25, 26] and even 3-D[27] hybrid particle simulations are now being applied.

4. Control of stimulated Raman scattering

Stimulated Raman scattering represents the growth of a scattered light wave plus an electron plasma wave. This is the instability which generated strong preheat in hohlraums irradiated with 1.06μm light using the Shiva Lasers. The principal strategy to control this instability is to keep the hohlraum plasma density sufficiently low, not drive the plasma too strongly (moderate $I\lambda_0^2$), and use laser beam smoothing. In NIF hohlraums driven with 0.35μm laser light, the plasma density within the hohlraum volume is about $0.1n_{cr}$ and the electron temperature is about 5keV during peak power. If we assume a Maxwellian distribution, the electron plasma wave associated with backscatter has a wave number $k\lambda_{De} \cong 0.5$ (λ_{De} is the electron Debye length) and is strongly Landau damped. The instability is then weakened and in general has a growth rate

$$\gamma = \frac{k^2 v_{os}^2}{8\omega_{sc}} \frac{\mathrm{Im}\,\varepsilon}{|\varepsilon|^2},$$

where ω_{sc} is the scattered light frequency and ε is the plasma dispersion function. In addition, the high energy electrons generated by the damped plasma wave have a modest temperature – only about 20 keV. Such electrons are not a preheat threat, due both to the self-shielding of the capsule and to the reduced probability that electrons generated in the hohlraum will transport to the capsule.

Some attention has been given to forward SRS, since the plasma wave is then weakly damped. Actually forward scatter at an angle has a larger growth rate than direct forward scatter in a homogeneous plasma. The angle for maximum growth rate is obtained by choosing the largest wavenumber plasma wave before Landau damping strongly onsets. In practice, the geometry of speckles and hot spots will constrain these angles to smaller values. Forward scattering is sensitive to plasma inhomogeneity and/or nonlinearly-induced modulations.[28, 29] Experiments to date[29] show low levels of SRS in the forward direction.

Until recently, the levels of SRS in the backward direction were thought to be low ($\leq 1\%$) in hohlraums[30] driven with 0.35μm light. This estimate was based on measurements of SRS light using a diode at about 30° from direct backscatter. However, more extensive diagnostics implemented for the plasma-scaling experiments showed that the Raman-scattered light was in fact quite collimated[9] back into the focusing lens. The levels are quite comparable to the SBS levels.

SRS is now routinely monitored in the backward direction. For high intensity $\left(\geq 5\times10^{15}\,\frac{W}{cm^2}\right)$ and/or high plasma density $(\geq 0.15 n_{cr})$, levels $\geq 20\%$ have been observed. Plasma density remains a very important control mechanism for SRS. For lower density, the phase velocity of the Raman-driven plasma wave is lower and both the backscatter and the heated electron temperature are less. In recent experiments[9] using plasmas with a density of about $0.1 n_{cr}$ irradiated with a 0.35μm light at an intensity of $2\times10^{15}\,\frac{W}{cm^2}$, the SRS levels are modest (~5%).

Recent experiments[31-34] have shed new light on the nonlinear behavior of SRS and on its rich interplay with SBS. An anti-correlation between SBS and SRS has been observed. In addition, experiments have demonstrated regimes in which the SRS back reflection increases as the ion wave damping increases. Such behavior is consistent with saturation of SRS by subsequent decay[35-37] of the

Raman-driven plasma wave into another plasma wave plus an ion wave (the so-called Langmuir decay instability). This subsequent decay has a threshold

$$\left(\frac{\delta n}{n}\right)^2 \sim 4k^2\lambda_{De}^2 \frac{\nu_i}{\omega_i}\frac{\nu_e}{\omega_{pe}},$$

where δn is the fluctuating plasma density associated with the Raman-driven plasma wave, k its wavenumber and λ_{De} the electron Debye length. Here $\nu_i(\omega_i)$ is the ion wave energy damping rate (frequency) and $\nu_e(\omega_{pe})$ is the electron plasma wave damping rate (frequency). As the ion wave damping rate increases, the Raman-generated plasma wave can grow to higher levels, giving larger scattering. A similar scaling might be obtained from saturation via a decay of the Raman plasma wave into a scattered light wave[37] plus an ion wave. Since the nonlinear behavior depends on the damping of the Raman-driven plasma wave, the experiments in general require consideration[38] of how the electron distribution function can be modified by either collisional absorption or by nonlocal electron transport. Clearly plasmas continue to exhibit a very rich, challenging, and sometimes perverse behavior.

5. Plasma scaling experiments

So-called plasma scaling experiments are a very essential part of the strategy to control laser plasma instabilities. Theory and computer simulations have identified key physical processes, important nonlinear consequences, and various techniques for instability control. However, quantitative calculations of the nonlinear levels and competition of these instabilities have not yet been achieved. What is possible is to use current lasers, such as Nova and OMEGA to test the instability levels in long scalelength plasmas with conditions as close as possible to those anticipated in NIF targets. Such experiments provide greater confidence as well as key data to test control mechanisms and stimulate the ongoing development of models.

The long scalelength experiments have been performed in both open and closed geometry. Let's here focus on some illustrative experiments in which large plasmas are created by irradiating gas bag[39] targets with nine Nova beams. A tenth interaction beam is then used to quantify the SRS and SBS levels as a function of irradiation and plasma conditions. Using such targets with the Nova laser, one can create, for example, a fairly uniform plasma with a length of about 2mm, a

density of about $10^{21}cm^{-3}$ (~$0.1n_{cr}$ for 0.35μm light), and an electron temperature of about 3keV. These conditions are close to those expected in the volume plasma in a NIF hohlraum. In the NIF target, the electron temperature is somewhat higher (4-5keV) and the plasma length less than a factor of two larger. In the scaling experiments, the intensity is varied to values both higher and lower than the nominal $2x10^{15}\frac{W}{cm^2}$ used in the NIF design. Various beam smoothing techniques are used, including random phase plates, SSD and the 4-color scheme.

As an example, the SRS reflectivity at the time of maximum plasma temperature (1ns) is shown in Figure 6 as a function of the intensity of the f/8 interaction beam. The different points refer to various beam smoothing schemes as noted in the caption. The reflectivity denotes the reflection into a cone up to 20° around the beam axis, although the reflection is concentrated into the original f/8 solid angle. Note that the SRS reflectivity is about 5% for an intensity of $2x10^{15}\frac{W}{cm^2}$ with either RPP or SSD. An SRS reflectivity up to nearly 15% is measured at higher intensities depending on the smoothing scheme.

The analogous most recent measurements for SBS back reflection show a similar reflectivity of about 5% for an intensity of $2x10^{15}\frac{W}{cm^2}$. However, experiments using gas bags with CO_2 or CD_2 gave an SBS reflectivity up to 35% for this intensity. Such results emphasize the role that light protons can play in reducing SBS, as discussed in Section 2. These results also suggest that in hohlraums most SBS comes from the low density Au plasma, where the ion wave damping is weak. Indeed, in experiments with a methane-filled hohlraum driven by a shaped Nova pulse, sizeable SBS backscatter has been observed.[40] The average reflectivity into a f/4 lens was about 10% in the standard (so-called scale-1) hohlraum (the peak reflectivity was ≥ 20%). However, the average SBS reflectivity in these hohlraums was much reduced to about 1.5% by using a laser beam smoothed with RPP and SSD. Further work is ongoing to better understand and control the stimulated scattering in hohlraums.

6. Summary

In conclusion, the control of laser plasma instabilities is one of the highest leverage issues in laser fusion research. Various techniques ranging from laser beam smoothing to plasma density and composition have been used to control the

instabilities in long scalelength plasmas. Plasma scaling experiments have shown tolerable instability levels for NIF-like parameters as well as a rich interplay between instabilities. Recent experiments[41] producing higher temperature hohlraums are also very encouraging. In these experiments, laser light was successfully absorbed in smaller hohlraums, i.e., even when the laser intensity was higher $\left(\sim 10^{16}\frac{W}{cm^2}\right)$ and the volume plasma became denser $\left(>\frac{1}{4}n_{cr}\right)$.

Progress continues on understanding the nonlinear levels and scalings. The various plasma waves are now being directly monitored in unprecedented detail. For example, Baldis and Lebaune are simultaneously measuring the temporal and spatial evolution of both electron plasma and ion acoustic waves. The modeling is also advancing. For example, the coupled evolution of SBS and filamentation including kinetic effects and plasma interpenetration is now being investigated using a three-dimensional particle ion, fluid electron code. Detailed comparisons are being made with experiments by Peter Young. Increased attention is focused on development of reduced descriptions: coupled differential equations describing the simultaneous evolution of electron and ion waves. Such models have successfully predicted features of plasma wave collapse and strong Langmuir turbulence as well as a regime in which SRS depends on ion wave damping. These models are now being developed to describe the two and three-dimensional instability evolution driven by structured laser beams.

Acknowledgments

This manuscript is based on an invited lecture given at the 1995 La Jolla Summer School on Plasma Physics and Technology. I am grateful for discussions with numerous colleagues, including S. Wilks, B. Afeyan, P. Young, B. Kirkwood, D. Montgomery, B. MacGowan, H. Baldis, E.M. Campbell, J. Moody, H. Vu, H. Rose, A. Schmitt, D. Hinkel, E. Williams, B. Lasinski, B. Langdon, and R. Berger. Work performed under the auspices of the U.S. Department of Energy by the Lawrence Livermore National Laboratory under Contract W-7405-ENG-48.

1. J. Lindl, Phys. Plasma **2**, 3933 (1995).

2. William L. Kruer, Phys. Fluids **B3**, 2356 (1991); see also William L. Kruer in Laser Plasma Interactions V, (Institute of Physics, Bristol, 1995), p. 27.

3. S.W. Haan, et al., Phys. Plasmas **2**, 2480 (1995).

4. H.A. Baldis, E.M. Campbell and W.L. Kruer, Physics of Laser Plasmas (North Holland, Amsterdam, 1991) p 361-434.

5. Y. Kato, et al., Phys Rev. Lett. **53**, 1057 (1984), X. Deng, X. Liang, Z. Chen, W. Yu and R. Ma Chin, J. Lasers **12** 257 (1985); R.H. Lehmberg and S.P. Obenschain, Opt. Commun. **46**, 27 (1983); S. Kkupsky et al., J. App. Phys. **66**, 3456 (1989).

6. H. A. Rose and D. F. Dubois, Phys. Fluids **B4**, 2521 (1992).

7. R.L. Berger, et al., Phys. Fluids **B5**, 2243 (1993).

8. A.J. Schmitt, Phys. Fluids **31** 3079 (1988).

9. B.J. MacGowan, B.B. Afeyan, et al., Phys. Plasmas **3**, 2029 (1996).

10. S.E. Cole, et al., Europhys. Lett. **10**, 31 (1989).

11. S.C. Wilks, P.E. Young, J. Hammer, M. Tabak and W.L. Kruer, Phys. Rev. Lett. **73**, 2994 (1994).

12. P.E. Young, J.H. Hammer, S.C. Wilks and W.L. Kruer, Phys. Plasma **2**, 2825 (1995).

13. S.G. Glendinning, L.V. Powers, R.L. Kauffman, O.L. Landen, B.B. Ress, G.F. Stone, L.J. Suter, A.L. Richard, "Measurements of Wall X-ray Emission Patterns in Gas-Filled Hohlraums", to be published; J.D. Moody, B.J.

MacGowan, D.E. Hinkel, W.L. Kruer, E.A. Williams, K.G. Estabrook, T.D. Shepard, R. Kirkwood, D.S. Montgomery and R.L. Berger, Phys. Rev. Letters **77**, 1294 (1996; Bruno Bauer, et al., to be published.

14. Harvey A. Rose, Phys. Plasmas (1995) **3**, 1709 (1996); D.E. Hinkel, E.A. Williams and C.H. Still, Phys. Rev. Letters **77**, 1298 (1996); W.L. Kruer and J.H. Hammer, Comments Plasma Phys. Cont. Fusion (in press); H.X. Vu, Phys. Plasmas (in press).

15. A.J. Schmitt and B.B. Afeyan, Bull. Am. Phys. Soc. **40**, 1824 (1995).

16. E.M. Epperlein, Phys. Rev. Lett. **65**, 2145 (1990).

17. B.C. Fried, Phys. Fluids **14**, 2338 (1971); H.X. Vu et al., Phys. Plasmas **1**, 3542 (1994); E.A. Williams et al., Phys. Plasmas **2**, 129 (1995).

18. S.C. Wilks et al., Phys. Rev. Letters **74** 25 (1995).

19. C.E. Clayton, C. Joshi, A. Yasuda, and F.F. Chen, Phys. Fluids **24**, 2312 (1981).

20. B.J. MacGowan et al., Lawrence Livermore National Laboratory, UCRL-LR 105821-95-4305-331 (1996).

21. J.C. Fernandez et al., Phys. Rev. E **53**, 2747 (1996).

22. W.L. Kruer, S.C. Wilks, B.B. Afeyan and R.K. Kirkwood, Phys. Plasmas **3**, 382 (1996); A. Maximov et al., Phys. Plasmas **3**, 1689 (1996).

23. R. Kirkwood et al., Phys. Rev. Letters **76**, 2065 (1996).

24. P.W. Rambo, S.C. Wilks and W.L. Kruer, Bull. Am. Phys. Soc. **40**, 1821 (1995).

25. H.X. Vu, J. Comp. Phys. **124**, 417 (1996).

26. B.I. Cohen et al., UCRL-JC 124922 (1996).

27. H.X. Vu, LA-UR-96-1816 (1996).

28. W.L. Kruer, Laser Interaction and Related Plasma Phenomena (Plenum, New York, 1993) Vol 10, p. 503.

29. S.H. Batha et al., Phys. Plasmas **1**, 1985 (1994).

30. R.L. Kauffman et al., UCRL-JC 117046 (1994); L.V. Powers et al, Phys. Rev. Letters **74**, 2957 (1995).

31. H. Baldis, C. Labaune, E. Shifano, N. Renard and A. Michard, Phys. Rev. Lett. **77**, 2957 (1996); H.A. Baldis et al., Phys. Rev. Letters **62**, 2829 (1989).

32. D.M. Montgomery et al., submitted to Phys. Rev. Letters (1996).

33. R.K. Kirkwood et al., Phys. Rev. Letters **77**, 2706 (1996).

34. J.C. Fernandez et al., Phys. Rev. Letters **77**, 2702 (1996).

35. S.J. Karttunen, Phys. Rev. A **23**, 2006 (1981), R.P. Drake and S.H. Batha, Phys. Fluids B **3**, 2936 (1991).

36. B. Bezzerides, D.F. Dubois, H.A. Baldis, Phys. Rev. Letters **70**, 2569 (1993); J.T. Kolber, W. Rozmus and V.T. Tikhonchuk, Phys. Fluids B **5**, 138 (1993).

37. K.L. Baker, Ph. D. Dissertation University of California, Davis (1996).

38. B.B. Afeyan, A.E. Chou, and W.L. Kruer, Submitted to Phys. Rev. Letters (1996).

39. J. Denavit and D. Phillion, Phys. Plasma **1**, 1971 (1994); D.H. Kalantar, et al., Phys. Plasmas **2**, 3161 (1995).

40. B.J. MacGowan et al., Private communication.

41. T.J. Orzechowski et al., Bull. Am. Phys. Soc. **41**, 1390 (1996).

Figure Captions:

Figure 1. The standard hohlraum for the National Ignition Facility.

Figure 2. a) The temporal profile of the laser power and contours of b) electron density, c) electron temperature, and d) laser intensity at time of peak power in a calculation of the NIF hohlraum.

Figure 3. A sketch of laser power versus energy, illustrating the parameter space available for ignition target design.

Figure 4. The reduction of SBS reflectivity versus proton fraction as computed in some simulations with a 1D particle ion - fluid electron code.

Figure 5. The measured reduction in SBS reflectivity versus hydrogen content in UCLA experiments with 10.6μm light.

Figure 6. The measured SRS reflectivity versus intensity from a gas bag target. The open squares denote 4-color, the blade squares 4-color with SSD, the gray codes 1-color and the black circles 1-color with SSD.

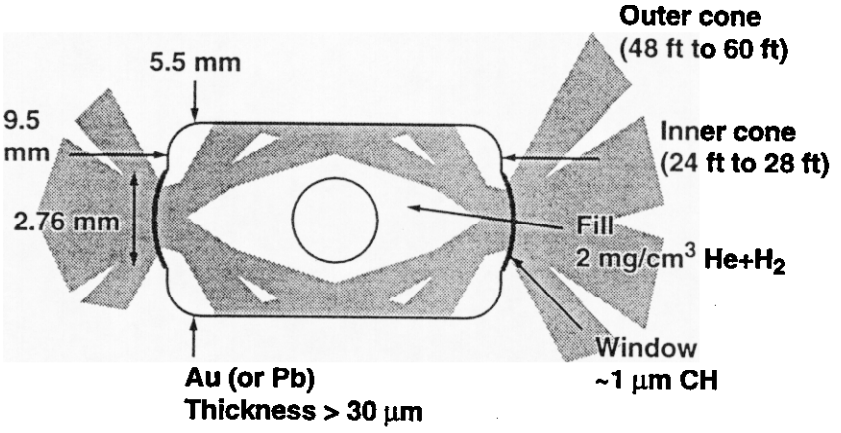

50-05-0494-1806 pb03

FIG 1

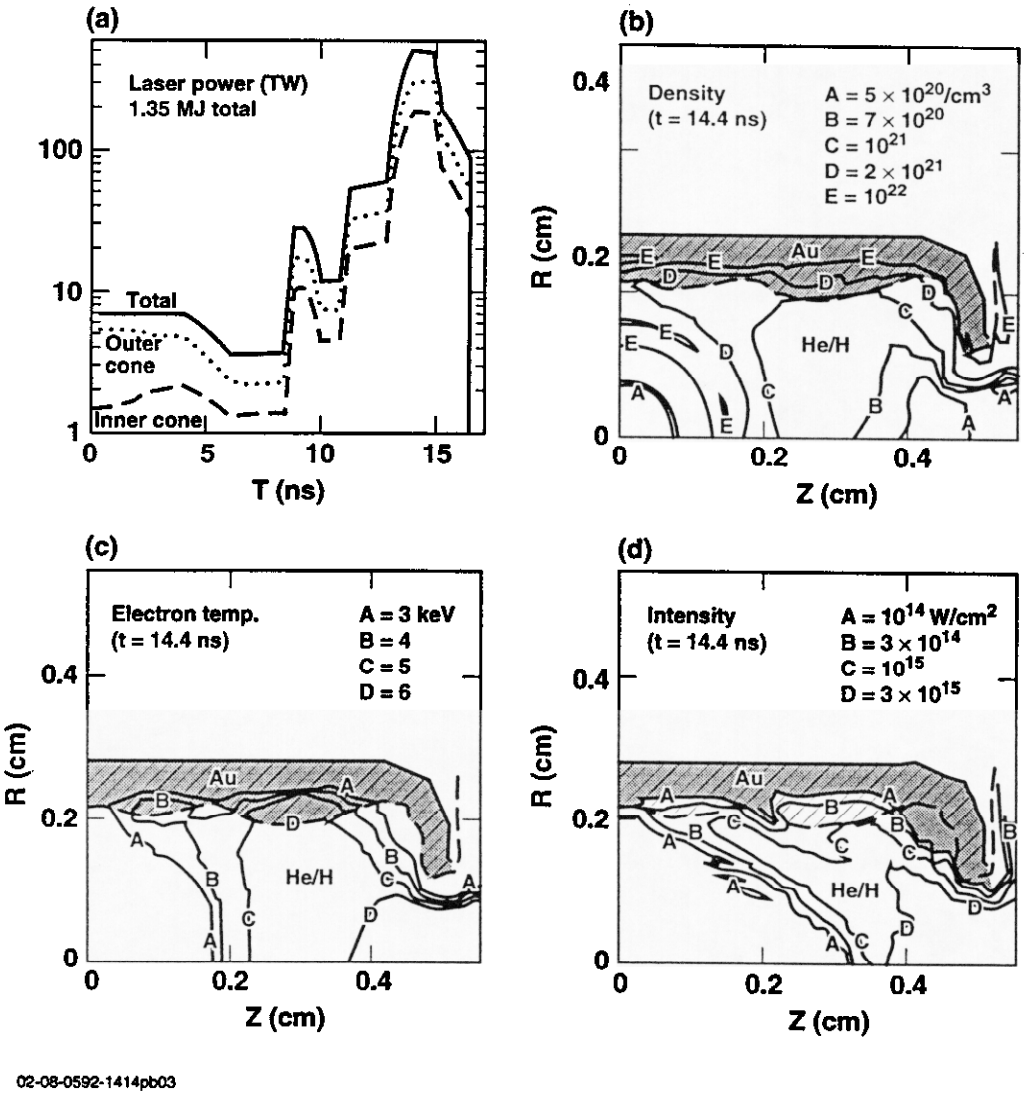

02-08-0592-1414pb03

FIG 2

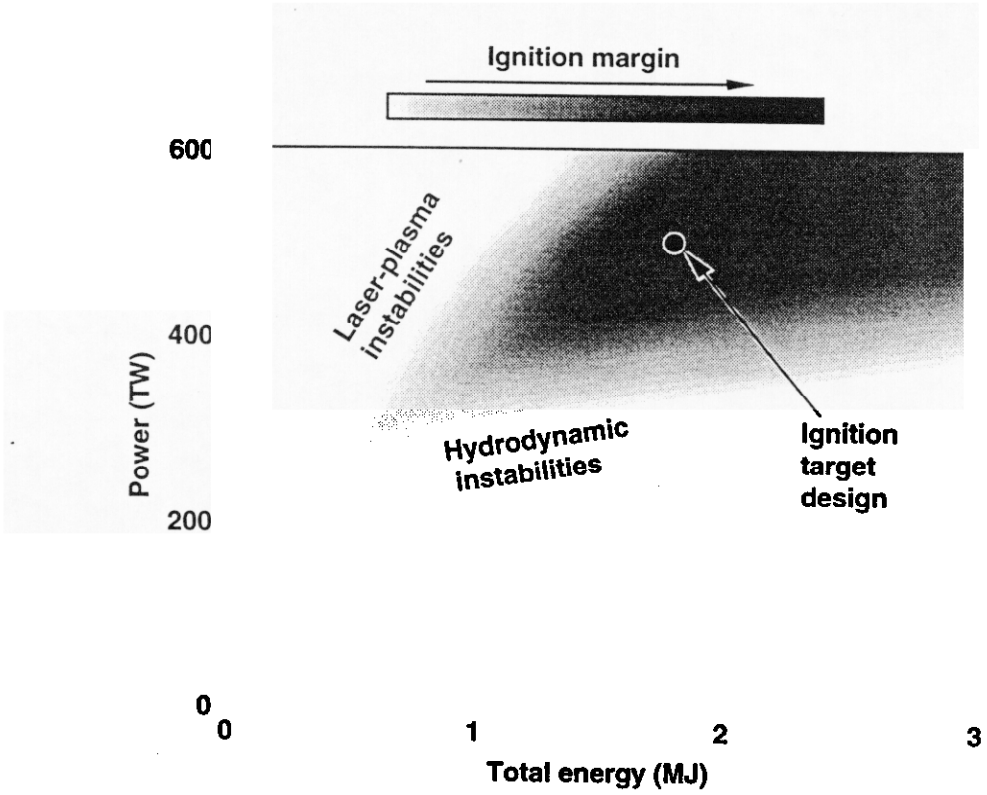

50-05-0494-1803pb03

FIG 3

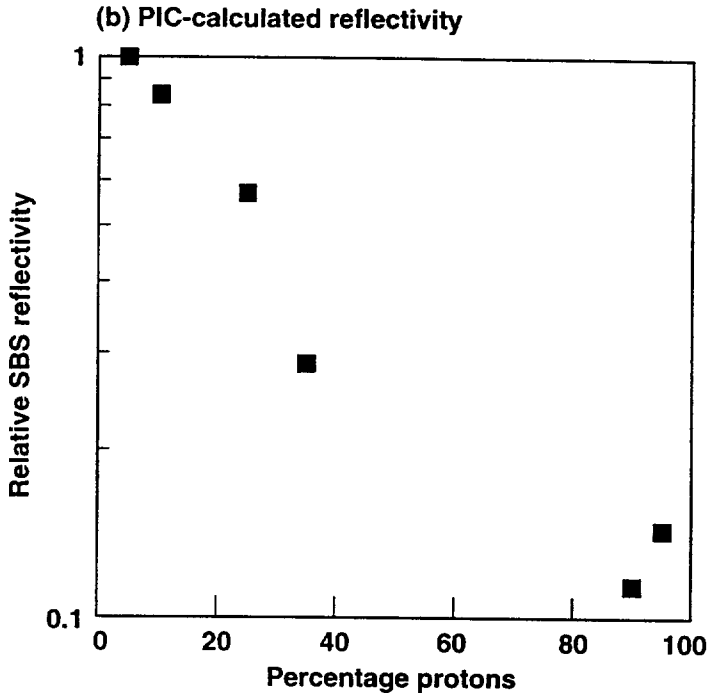

20-07-1095-2442pb02

FIG 4

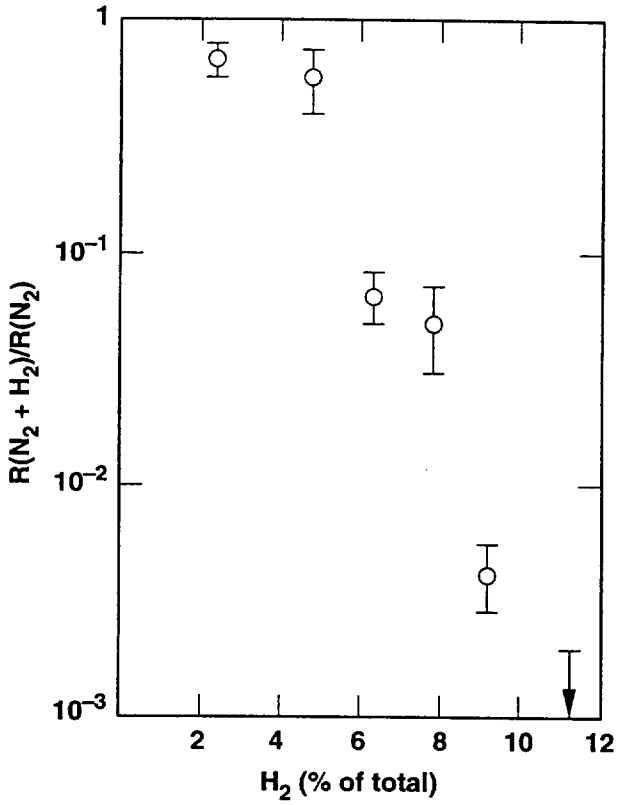

50-01-0994-3429pb01

20WLK/gbh

FIG 5

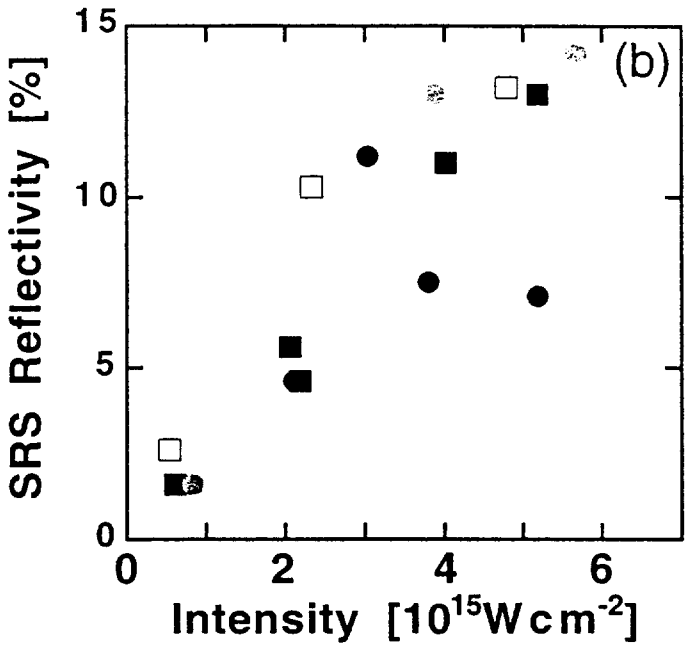

FIG 1

Technical Information Department • **Lawrence Livermore National Laboratory**
University of California • Livermore, California 94551